J|A|C|S

JOURNAL OF THE AMERICAN CHEMICAL SOCIETY

Amine-Assisted Synthesis of Concave Polyhedral Platinum Nanocrystals Having {411} High-Index Facets

Xiaoqing Huang, Zipeng Zhao, Jingmin Fan, Yueming Tan, and Nanfeng Zheng*

State Key Laboratory for Physical Chemistry of Solid Surfaces and Department of Chemistry, College of Chemistry and Chemical Engineering, Xiamen University, Xiamen 361005, China

S *Supporting Information*

ABSTRACT: High-index surfaces of a face-centered cubic metal (e.g., Pd, Pt) have a high density of low-coordinated surface atoms and therefore possess enhanced catalysis activity in comparison with low-index faces. However, because of their high surface energy, the challenge of chemically preparing metal nanocrystals having high-index facets remains. We demonstrate in this work that introducing amines as the surface controller allows concave Pt nanocrystals having {411} high-index facets to be prepared through a facile wet-chemical route. The as-prepared Pt nanocrystals display a unique octapod morphology with {411} facets. The presence of high-index {411} exposed facets endows the concave Pt nanocrystals with excellent electrocatalytic activity in the oxidation of both formic acid and ethanol.

Because of their broad use in catalysis, photonics, electronics, plasmonics, optical sensing, biological labeling, imaging, and photothermal therapy, the controlled synthesis of noble-metallic nanocrystals with uniform geometries has been a research theme for decades.[1−4] The properties of noble-metallic nanocrystals are strongly determined by their size, shape, and surface structure.[5−10] In the past several years, increasing attention has been paid to the fabrication of metallic nanoparticles enclosed by high-index facets.[11−20] As a result of the high density of low-coordinated atoms in the forms of atomic steps and kinks, high-index facets are generally more active toward specific reactions than low-index planes that are composed of closely packed surface atoms.[21−23]

However, because of their high surface energy, preserving high-index facets during the growth of nanocrystals remains a significant challenge. A unique electrochemical method has recently been developed by Sun and co-workers[11−13,23] for the preparation of Pt and Pd nanocrystals that are enclosed by high-index {hk0} facets and therefore display superior electrocatalytic performance. Several groups have achieved the wet-chemical synthesis of Au nanocrystals with high-index facets.[14−17] More recently, catalytic Au−Pd core−shell nanocrystals having high-index facets were also fabricated by using Au nanocrystals as seeds.[18−20] Because it is easily scaled up, chemical synthesis is more desirable than electrochemical methods for preparing high-index faceted metallic nanocrystals for possible applications. Unfortunately, only high-index faceted Au and Au−Pd nanocrystals have been chemically prepared to date.[14−20]

In our previous studies, we successfully prepared various noble-metallic nanostructures (e.g., Pd/Pt nanocubes, Pd concave polyhedra, Pd nanosheets) by the selective use of specific small molecules (e.g., I⁻, HCHO, CO).[24−28] These results inspired us to investigate whether it is possible to use a similar strategy to synthesize metallic nanocrystals with high-index facets. Herein we demonstrate that concave Pt nanocrystals having high-index {411} facets can be prepared by the selective use of amine via a facile wet-chemical method. The as-prepared concave Pt nanocrystals exhibit far better catalytic activity than commercial Pt black and Pt/C (E-TEK) catalysts.

The concave Pt nanocrystals with high-index {411} facets were solvothermally prepared by reduction of hexachloroplatinic acid at 160 °C for 11 h in a Teflon-lined stainless steel autoclave with a capacity of 20 mL using poly(vinylpyrrolidone) (PVP) as the surfactant in the presence of methylamine (see the Supporting Information for details). The resulting products were collected by centrifugation and washed several times with ethanol and acetone.

The as-prepared Pt nanocrystals were first characterized by scanning electron microscopy (SEM). As shown in the SEM images in Figure 1a and Figure S1 in the Supporting Information, the product consisted of uniform four-armed starlike particles with a yield above 90%. The apex angle of each arm was measured to be 53°. In the SEM image at a higher magnification, the four arms are much brighter than the center region of the starlike particles (Figure 1b), indicating the possible presence of a concave feature in the particles. To better visualize the three-dimensional structure of the nanocrystals, we tilted the sample away from the direction perpendicular to the electron beam, after which the concave features became more notable. The as-prepared concave particles are essentially octapods having eight trigonal pyramidal arms (Figure 1c). In the SEM image before tilting, most of the particles were observed as four-armed stars simply because they prefer to lie flat on the substrate using four of their eight arms. When hindered by neighboring particles, some octapods were able to settle on the substrate using only two arms (Figure 1d), allowing direct three-dimensional visualization of the concave particles. At the core of the octapod, basins surrounded by every four trigonal-pyramidal arms can be observed. On the basis of these observations, we have proposed a structural model (inset in Figure 1d) for the as-prepared Pt nanocrystals. According to the apex angle of the trigonal pyramidal arms, we can also infer that the exposed facets of the
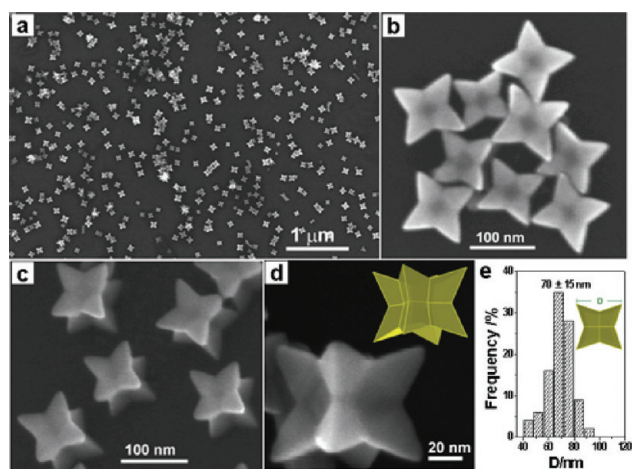
Figure 1. (a—c) Typical (a) large-area, (b) enlarged, and (c) tilted SEM images of the as-prepared concave Pt nanocrystals. (d) High-magnification SEM image of a single concave Pt nanocrystal. The top-right inset shows an ideal geometrical model of the concave Pt nanocrystal with the same orientation as the nanocrystal in the SEM image. (e) Size distribution of the as-prepared concave Pt nanocrystals.
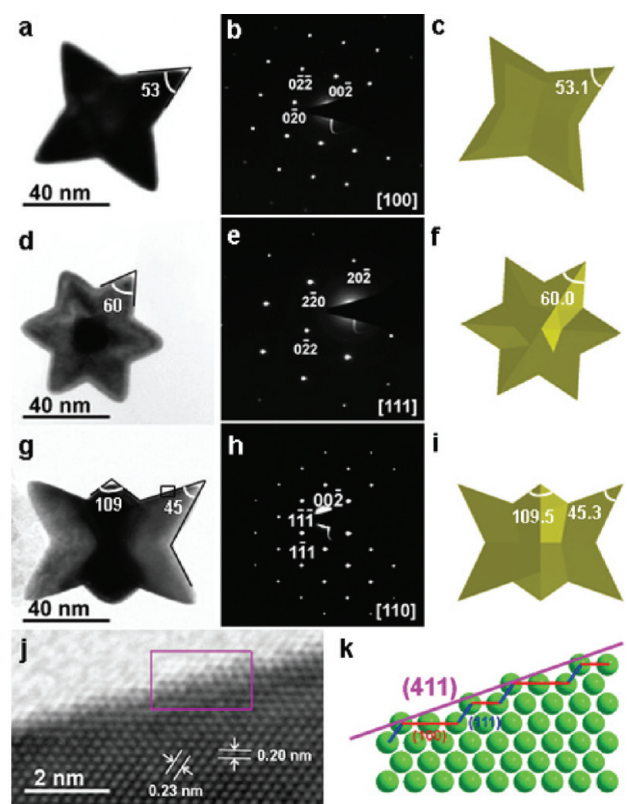

Figure 2. (a, d, g) TEM images, (b, e, h) SAED patterns, and (c, f, i) geometric models of individual concave Pt nanocrystals oriented along the (a—c) [100], (d—f) [111], and (g—i) [110] directions. (j) HRTEM image of the region indicated by the box in (g). (k) Atomic model corresponding to the region indicated by the box in (j).

trigonal pyramidal arms are {411}. The structure can be better described by excavating out a tetragonal pyramid from each square (100) face of a cube. Each cut-out pyramid has a square (100) base face and four exposed (411) faces passing through the

four corners of the excavated (100) square face (see Figure S2 for detailed models). Overall, an octapod particle has 24 identical kite-shaped {411} faces, each of which is composed of two coplanar isosceles triangles with apex angles of 50.5 and 86.6° sharing the same base. The as-prepared Pt nanocrystals have an average apex-to-apex diameter of ~70 nm (Figure 1e).

To confirm the proposed structure, the concave Pt nanocrystals were also thoroughly characterized by transmission electron microscopy (TEM). The proposed structure was first confirmed by a set of tilted TEM images of the concave nanocrystals (Figure S3). Both high-resolution TEM (HRTEM) and selected-area electron diffraction (SAED) measurements on individual star-shaped Pt nanocrystals clearly demonstrated their single-crystalline nature. Coupled SAED and HRTEM analyses determined the zone axes of the crystals together with their lattice parameters, allowing an unambiguous structural identification of the crystals. Figure 2 presents representative TEM images, the corresponding SAED patterns, and oriented geometric models of the Pt octapods viewd along three different zone axes (i.e., [100], [111], and [110]). Similar to the SEM sample, most of the particles lay flat on the TEM substrate and were present as four-armed stars (Figure 2a and Figure S4). The SAED pattern of an individual four-armed starlike crystal (Figure 2b) was indexed to the [100] zone axis of face-centered cubic Pt. The contour of the nanocrystal also fit well with the proposed octapod model in the [100] projection (Figure 2c). As shown in Figure 2d–f, a typical perfect hexagram-like particle has an orientation along the [111] zone axis, as also confirmed by the SAED analysis. The apex angles were measured to be 53 and 60° for the crystals oriented along [100] and [111], respectively, consistent with the theoretical values from the geometric model.

As shown in Figure 2g—i, when projected along [110], the Pt octapods appeared as elongated six-armed stars with four long and two short arms. The apex angles for the long and short arms were measured to be 45 and 109°, respectively. When octapod crystals were oriented along the [110] zone axis, some of their (411) faces were driven parallel to the TEM beam, allowing the direct observation of the atomic arrangement by HRTEM. As illustrated in Figure 2j, ([2n − 1],1,1) steps [e.g., (311), (511)] made of subfacets of (111) and (100) planes can clearly be observed in the (411) surface oriented in the [110] direction, matching the atomic model well [Figure 2k; see Figure S5 for the detailed structure of a (411) surface].

In the synthesis of the concave Pt nanocrystals, the use of the amine was essential. The reactions in the absence of amine yielded Pt nanocrystals with mixed morphologies (e.g., cubes, cuboctahedra) (Figure S6). The perfect Pt octapod nanocrystals were obtained only by supplying a certain amount of methylamine (0.10 mL of 30% methylamine) to the 10 mL reaction solution. When the amount of methylamine was reduced to 0.04 mL, the degree of concavity (defined in Figure S7) of the obtained nanocrystals was significantly reduced (Figure S8). The concave feature was hardly even observed in the products when the amount of methylamine was further reduced to 0.02 mL. The less concave the particles were, the smaller the ratio of {411} to {100} facets was. Reducing the methylamine supply decreased the degree of concavity, suggesting that the essential role of methylamine in the formation of the octapod nanocrystals might originate from the selective binding of methylamine on the high-index {411} facets of Pt during growth. Fourier transform IR (FT-IR) spectroscopy was used to detect the binding of methylamine on the as-made Pt nanocrystals. All of the typical
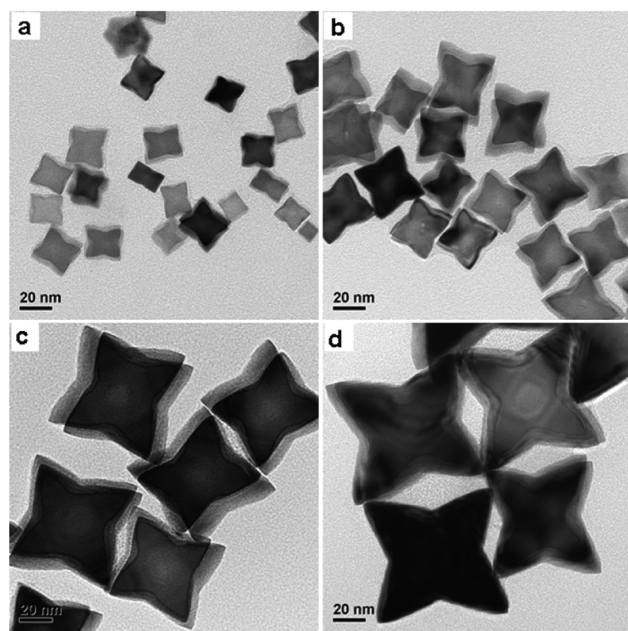
Figure 3. TEM images of the concave Pt nanocrystals produced after (a) 3.0, (b) 5.0, (c) 8.0, and (d) 11 h of reaction.

Figure 4. CV curves for electro-oxidation of (a) formic acid and (b) ethanol by the as-prepared concave Pt nanocrystals, commercial Pt black, and Pt/C (E-TEK). The formic acid oxidation was recorded in $0.5\ M\ H_2SO_4 + 0.25\ M\ HCOOH$ solution at a scan rate of 50 mV/s. The ethanol oxidation was recorded in $0.1\ M\ HClO_4 + 0.1\ M\ CH_3CH_2OH$ solution at a scan rate of 50 mV/s.

absorption bands of methylamine were displayed in the IR spectrum of the purified Pt nanocrystals (Figure S9). This result supports the conclusion that methylamine was indeed present on the surface of the as-made Pt nanocrystals. Interestingly, when methylamine was substituted with other amines (i.e., ethylamine, butylamine, 4-methylpiperidine, trimethylamine), the reactions also yielded concave nanocrystals (Figure S10). In contrast, only small cubic or cuboctahedral particles were obtained from reactions in which methylamine was substituted with methanol (Figure S11), indicating the correlation of the formation of concave Pt particles with the amino group. In the synthesis, we also found that the use of PVP is important in obtaining concave Pt nanocrystals with good dispersivity but not essential for the formation of concave particles. The reactions in the absence of PVP also gave concave particles, but they were heavily aggregated (Figure S12), suggesting that the main role of PVP is to protect and disperse the Pt particles.

Since methylamine was the most essential for the formation of concave nanocrystals and it was supplied once at the very beginning, one can expect that the concave feature would be concomitant with the whole growth process. TEM observations of the particles produced at different growth times confirmed this expectation. As shown in Figure 3, the size of the Pt particles grew with the reaction time. The average apex-to-apex diameters of the nanocrystals formed at 3, 5, 8, and 11 h were 19, 31, 59, and 70 nm, respectively. After 11 h, the reaction was complete, and the size of the Pt octapods did not change further. Although the size of the particles increased with the reaction time, the concave feature was maintained throughout the reaction (Figure S13). Together with the FT-IR characterization, this result suggests that the coordination of amine, which helps to stabilize the low-coordinated Pt sites, is the main reason why the high-index {411} facets can be preserved during the synthesis. It is also worth noting that the concave Pt nanocrystals could be readily prepared under nonsolvothermal conditions. Reactions in a flask attached
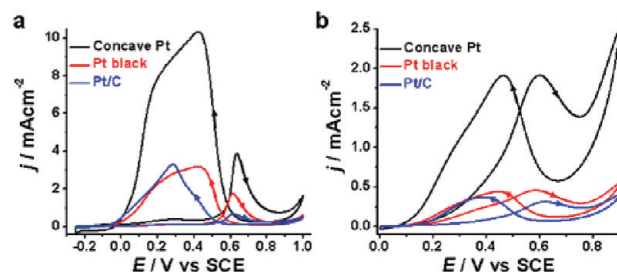
to a Schlenk line under a constant N_2 flow also yielded concave nanocrystals (Figure S14).

Since the Pt(411) surface has a high density of atomic steps, the as-prepared concave Pt nanocrystals should have enhanced catalysis activities. To demonstrate their structural advantage in catalysis, we chose to examine their use in the electrocatalytic oxidation of formic acid and ethanol. Commercial Pt black (Figure S15) and Pt/C (E-TEK) (Figure S16) catalysts were used as references for comparison. Figure 4 compares the cyclic voltammetry (CV) curves for the electro-oxidations of formic acid and ethanol on the three different catalysts. The current densities were normalized to the electrochemically active surface areas (ECSAs), which were obtained from the electric charge of hydrogen adsorption/desorption on Pt surfaces. Such normalization allowed the current density to be used directly to compare the catalytic activities of the three catalysts. The peak current densities of formic acid oxidation at 0.61 V (vs SCE) in the forward (positive) potential scan were 3.9, 1.7, and 0.7 mA/cm^2 on the concave Pt nanocrystals, commercial Pt black, and Pt/C catalyst, respectively. The activity of the concave Pt nanocrystals was 2.3 and 5.6 times greater than those of commercial Pt black and Pt/C, respectively. Similar behavior was also found in the electro-oxidation of ethanol, for which the concave Pt nanocrystals showed the best activity, 4.2 and 6.0 times greater than those of commercial Pt black and Pt/C, respectively, at 0.60 V (vs SCE). The results clearly demonstrate that the presence of the {411} facets of the concave Pt nanocrystals endows them with outstanding electrocatalytic activity. Moreover, the concave Pt nanocrystals displayed excellent stability during the electrochemical measurements (Figures S17 and S18). TEM measurements revealed that after the electrocatalysis experiments, the nanocrystals still nicely maintained their concave structure (Figure S19).

In summary, we have successfully prepared concave Pt nanocrystals enclosed by both high-index {411} and {100} facets via a facile wet-chemical route. The use of amine was demonstrated to be the most essential for the formation of the concave nanocrystals. Because of the presence of the high-index {411} exposed facets, the as-prepared concave Pt nanocrystals exhibit higher electrocatalytic activity per unit surface area than either commercial Pt black or Pt/C in the electro-oxidations of formic acid and ethanol. Further studies are still required in order to understand fully how small molecules (amines in this case) determine the formation of high-index Pt facets.

■ ASSOCIATED CONTENT

ⓢ Supporting Information. Experimental details and additional data. This material is available free of charge via the Internet at http://pubs.acs.org.

■ AUTHOR INFORMATION

Corresponding Author
nfzheng@xmu.edu.cn

■ ACKNOWLEDGMENT

■ REFERENCES

(1) Burda, C.; Chen, X. B.; Narayanan, R.; El-Sayed, M. A. *Chem. Rev.* **2005**, *105*, 1025.

(2) Rosi, N. L.; Mirkin, C. A. *Chem. Rev.* **2005**, *105*, 1547.

(3) Tao, A. R.; Habas, S.; Yang, P. D. *Small* **2008**, *4*, 310.

(4) Xia, Y.; Xiong, Y. J.; Lim, B.; Skrabalak, S. E. *Angew. Chem., Int. Ed.* **2009**, *48*, 60.

(5) Habas, S. E.; Lee, H.; Radmilovic, V.; Somorjai, G. A.; Yang, P. D. *Nat. Mater.* **2007**, *6*, 692.

(6) Tsung, C. K.; Kuhn, J. N.; Huang, W. Y.; Aliaga, C.; Hung, L. I.; Somorjai, G. A.; Yang, P. D. *J. Am. Chem. Soc.* **2009**, *131*, 5816.

(7) Bratlie, K. M.; Lee, H.; Komvopoulos, K.; Yang, P. D.; Somorjai, G. A. *Nano Lett.* **2007**, *7*, 3097.

(8) Mulvihill, M. J.; Ling, X. Y.; Henzie, J.; Yang, P. D. *J. Am. Chem. Soc.* **2010**, *132*, 268.

(9) Xiong, Y. J.; Wiley, B.; Xia, Y. N. *Angew. Chem., Int. Ed.* **2007**, *46*, 7157.

(10) Wang, C.; Daimon, H.; Onodera, T.; Koda, T.; Sun, S. H. *Angew. Chem., Int. Ed.* **2008**, *47*, 3588.

(11) Tian, N.; Zhou, Z. Y.; Sun, S. G.; Ding, Y.; Wang, Z. L. *Science* **2007**, *316*, 732.

(12) Tian, N.; Zhou, Z. Y.; Yu, N. F.; Wang, L. Y.; Sun, S. G. *J. Am. Chem. Soc.* **2010**, *132*, 7580.

(13) Zhou, Z. Y.; Huang, Z. Z.; Chen, D. J.; Wang, Q.; Tian, N.; Sun, S. G. *Angew. Chem., Int. Ed.* **2010**, *49*, 411.

(14) Ma, Y. Y.; Kuang, Q.; Jiang, Z. Y.; Xie, Z. X.; Huang, R. B.; Zheng, L. S. *Angew. Chem., Int. Ed.* **2008**, *47*, 8901.

(15) Ming, T.; Feng, W.; Tang, Q.; Wang, F.; Sun, L. D.; Wang, J. F.; Yan, C. H. *J. Am. Chem. Soc.* **2009**, *131*, 16350.

(16) Zhang, J. A.; Langille, M. R.; Personick, M. L.; Zhang, K.; Li, S. Y.; Mirkin, C. A. *J. Am. Chem. Soc.* **2010**, *132*, 14012.

(17) Kim, D. Y.; Im, S. H.; Park, O. O. *Cryst. Growth Des.* **2010**, *10*, 3321.

(18) Lu, C. L.; Prasad, K. S.; Wu, H. L.; Ho, J. A. A.; Huang, M. H. *J. Am. Chem. Soc.* **2010**, *132*, 14546.

(19) Yu, Y.; Zhang, Q.; Liu, B.; Lee, J. Y. *J. Am. Chem. Soc.* **2010**, *132*, 18258.

(20) Wang, F.; Li, C. H.; Sun, L. D.; Wu, H. S.; Ming, T.; Wang, J. F.; Yu, J. C.; Yan, C. H. *J. Am. Chem. Soc.* **2011**, *133*, 1106.

(21) Somorjai, G. A. *Science* **1985**, *227*, 902.

(22) Somorjai, G. A.; Blakely, D. W. *Nature* **1975**, *258*, 580.

(23) Tian, N.; Zhou, Z. Y.; Sun, S. G. *J. Phys. Chem. C* **2008**, *112*, 19801.

(24) Huang, X. Q.; Zheng, N. F. *J. Am. Chem. Soc.* **2009**, *131*, 4602.

(25) Huang, X. Q.; Tang, S. H.; Zhang, H. H.; Zhou, Z. Y.; Zheng, N. F. *J. Am. Chem. Soc.* **2009**, *131*, 13916.

(26) Huang, X. Q.; Zhang, H. H.; Guo, C. Y.; Zhou, Z. Y.; Zheng, N. F. *Angew. Chem., Int. Ed.* **2009**, *48*, 4808.

(27) Wu, B. H.; Zheng, N. F.; Fu, G. *Chem. Commun* **2011**, *47*, 1039.

(28) Huang, X. Q.; Tang, S. H.; Mu, X. L.; Dai, Y.; Chen, G. X.; Zhou, Z. Y.; Ruan, F. X.; Yang, Z. L.; Zheng, N. F. *Nat. Nanotechnol.* **2011**, *6*, 28.